Supplement of Earth Syst. Dynam., 14, 399–412, 2023
https://doi.org/10.5194/esd-14-399-2023-supplement

Earth System Dynamics
Open Access

Supplement of

How does the phytoplankton–light feedback affect the marine N_2O inventory?

Sarah Berthet et al.

Correspondence to: Sarah Berthet (sarah.berthet@meteo.fr)

This Supplement includes:

A. Supporting text

N$_2$O parameterization in PISCESv2

As described by Aumont et al. (2015), PISCESv2 models five limiting nutrients for phytoplankton growth: nitrate and ammonium, phosphate, silicate and iron. The phosphate, nitrate-ammonium nutrient pools are not really independent in PISCESv2, as they are linked by a constant Redfield ratio across all modelled organic compartments. Redfield ratios are set to 122:16:1 for C:N:P following Takahashi et al. (1985) and the -O:C ratio is set to 1.34 (Kortzinger et al., 2001).

For our study the marine N$_2$O cycle described below was added to PISCESv2. In the ocean, N$_2$O production and consumption are driven by marine bacteria in slightly oxygenated waters. N$_2$O can occur as a by-product during microbial nitrification and as an intermediate product during denitrification (Freing et al., 2012). The oxic-anoxic interface above oxygen minimum zones provides appropriate conditions to enable N$_2$O production (Ji et al., 2018). In the absence of oxygen, nitrate (NO_3^-) is the next preferred electron acceptor for respiration after oxygen according to the electrochemical series (Lam and Kuypers, 2011). Denitrification has been shown to be the dominant process for N$_2$O production in the southern (Ji et al., 2015, 2018) and northern (Ji et al., 2018) part of the Pacific oxygen minimum zone. While nitrification is typically assumed to be an aerobic process, substantial suboxic nitrification has also been reported in many of the world ocean's major suboxic zones.

The bacterial pool is not yet explicitly modelled in PISCESv2. Processes of N_2O production like nitrification or denitrification are not formally expressed, and PISCESv2 diagnoses their effects from specific environmental conditions. A modelling approach relying on the indirect representation of the N_2O yield is rather common in present Earth system models due to the complexity of processes involved (Battaglia and Joos, 2018). For example, in MPI-ESM 1-2-LR (Ilyina et al., 2013) and MIROC-ES2L (Hajima et al., 2020), two of the few other Earth system models simulating marine N_2O emissions in CMIP6 (Séférian et al., 2020), the production of N_2O is mainly linked to the consumption of oxygen (O_2) during remineralization of organic matter.

In PISCESv2 it is assumed that the distribution of nitrifying bacteria in the model is ubiquitous in the ocean interior, that is wherever there is export of organic matter to depth the model simulates nitrification, consuming ammonium and producing nitrate (Martinez-Rey et al., 2015). Nitrification is particularly enhanced in the absence of light, whereas oxygen levels should be above the suboxic threshold of 1 µmol L^{-1}. Denitrification is computed in the model where dissolved oxygen concentration falls below 5 µmol L^{-1}, which defines suboxic waters (Cocco et al., 2013; Bopp et al., 2013).

At each grid point below 100 m depth (as N_2O production is inhibited by light), a unitless function $f(O_2)$ depending on the oxygen concentration $[O_2]$ (in µmol L^{-1}) is computed following:

$$\left.\begin{array}{l} f([O_2] < 1\ \mu mol\ L^{-1}) = [O_2] \\ f(1\ \mu mol\ L^{-1} \leq [O_2] \leq 5\ \mu mol\ L^{-1}) = 1 \\ f([O_2] > 5\ \mu mol\ L^{-1}) = 0.7*\exp(-0.1*([O_2] - 5)) + 0.3*\exp(-0.01*([O_2] - 5)) \end{array}\right\} \quad (1)$$

$f(O_2)$ allows to evaluate the suboxic production of N_2O based on Martinez-Rey et al. (2015):

$$[N_2O]_{suboxic} = \alpha + \beta * f(O_2) \quad (2)$$

with α, being the nitrification coefficient for N_2O background production equal to 10^{-4} mol N_2O per mol O_2 consummed. β, is the denitrification coefficient which scales the oxygen-dependent function. It is equal to 30 10^{-4} mol N_2O per mol O_2 consummed.

The local trend of nitrous oxide concentration $[N_2O]$ is finally evaluated by Eq. (3) at each time step as:

$$\begin{aligned} d[N_2O]/dt = \; & [N_2O]_{suboxic} * zolimit * o2ut && (3.1)\ \text{remineralization} \\ & - sink_{N2O} * [N_2O] && (3.2)\ \text{sink term} \\ & + [N_2O]_{suboxic} * zonitr * o2nit && (3.3)\ \text{nitrification} \\ & + [N_2O]_{suboxic} * zgrazing * o2ut && (3.4)\ \text{grazing} \end{aligned}$$

where in the first term (3.1) zolimit accounts for ammonification in oxic waters through oxygen consumption during the remineralization of the organic matter at the o2ut ratio of 133/122. In the second term (3.2) $sink_{N2O}$ is the N_2O sink term coefficient corresponding to the N_2O consumed under anoxic conditions by denitrification at a rate of $7.12\ 10^{-4}\ d^{-1}$. The third term (3.3) represents the part of N_2O concentration produced as an intermediate product of nitrification at a o2nit ratio of 32/122. The last term (3.4) produces N_2O by grazing of the remnant organic matter.

The N_2O partial pressure difference across the air-sea interface (sea-to-air Dpn2o; in atm) is then computed based on

$$Dpn2o = [N_2O]_{surface} / solub_{N2O} - pn2o \qquad (4)$$

with pn2o, the atmospheric partial pressure of N_2O in ppb, and $solub_{N2O}$ the N_2O solubility in mol/m^3 which depends on in-situ temperature and practical salinity following the formulation of Weiss and Price (1980).

Finally sea-to-air N_2O fluxes ($mol/m^2/s$) are inferred based on Wanninkhof (1992; 2014):

$$N_2O\_flux = Dpn2o * solub_{N2O} * Kg_{N2O} \qquad (5)$$

with Kg_{N2O} being the piston velocity for N_2O (m/s), which depends on wind speed, ice fraction and temperature.

References

Aumont, O., Ethé, C., Tagliabue, A., Bopp, L., and Gehlen, M.: PISCES-v2: An ocean biogeochemical model for carbon and ecosystem studies. Geoscientific Model Development, 8, 2465–2513, 2015.

Battaglia, G., and Joos, F.: Marine N2O emissions from nitrification and denitrification constrained by modern observations and projected in multimillennial global warming simulations. Global Biogeochemical Cycles, 32, 92–121. https://doi.org/10.1002/2017GB005671, 2018.

Bopp, L., Resplandy, L., Orr, J. C., Doney, S. C., Dunne, J. P., Gehlen, M., Halloran, P., Heinze, C., Ilyina, T., Séférian, R., Tjiputra, J., and Vichi, M.: Multiple stressors of ocean ecosystems in the 21st century: projections with CMIP5 models, Biogeosciences, 10, 6225–6245, https://doi.org/10.5194/bg-10-6225-2013, 2013.

Cocco, V., Joos, F., Steinacher, M., Frölicher, T. L., Bopp, L., Dunne, J., Gehlen, M., Heinze, C., Orr, J., Oschlies, A., Schneider, B., Segschneider, J., and Tjiputra, J.: Oxygen and indicators of stress for marine life in multi-model global warming projections, Biogeosciences, 10, 1849–1868, https://doi.org/10.5194/bg-10-1849-2013, 2013.

Freing, A., Wallace, D. W. R., and Bange, H. W.: Global oceanic production of nitrous oxide. Philos. Trans. R. Soc. London Ser. B, **367**, 1245–1255, 2012.

Hajima, T., Watanabe, M., Yamamoto, A., Tatebe, H., Noguchi, M. A., Abe, M., Ohgaito, R., Ito, A., Yamazaki, D., Okajima, H., Ito, A., Takata, K., Ogochi, K., Watanabe, S., and Kawamiya, M.: Development of the MIROC-ES2L Earth system model and the evaluation of biogeochemical processes and feedbacks, Geosci. Model Dev., 13, 2197–2244, https://doi.org/10.5194/gmd-13-2197-2020, 2020.

Ilyina, T., Six, K. D. , Segschneider, J., Maier-Reimer, E., Li, H., and Núñez-Riboni, I.: Global ocean biogeochemistrymodel HAMOCC: Model architecture and performance as component of the MPI-Earth system model in different CMIP5 experimental realizations,J.Adv.Model.EarthSyst.,5, 287–315, doi:10.1029/2012MS000178, 2013.

Ji, Q., Babbin, A. R., Jayakumar, A., Oleynik, S., and Ward, B. B.: Nitrous oxide production by nitrification and denitrification in the Eastern Tropical South Pacific oxygen minimum zone, Geophys. Res. Lett., 42, 10,755–10,764, doi:10.1002/2015GL066853, 2015.

Ji, Q., Buitenhuis, E., Suntharalingam, P., Sarmiento, J. L., and Ward, B. B. Global nitrous oxide production determined by oxygen sensitivity of nitrification and denitrification. Global Biogeochemical Cycles, 32, 1790–1802. https://doi.org/10.1029/2018GB005887, 2018.

Kortzinger, A., Hedges, J. I., and Quay, P. D.: Redfield ratios revisited: removing the biasing effect of anthropogenic CO2, Limnol. Oceanogr., 46, 964–970, 2001.

Lam, P., and Kuypers, M.: Microbial Nitrogen Cycling Processes in Oxygen Minimum Zones, Annual Review of Marine Science 3:1, 317-345, doi:10.1146/annurev-marine-120709-142814, 2011.

Martinez-Rey, J., Bopp, L., Gehlen, M., Tagliabue, A., and Gruber, N.: Projections of oceanic N_2O emissions in the 21st century using the IPSL Earth system model, Biogeosciences, 12, 4133–4148, https://doi.org/10.5194/bg-12-4133-2015, 2015.

Séférian, R., Berthet, S., Yool, A., Palmiéri, J., Bopp, L., Tagliabue, A., Kwiatkwski, L., Aumont, O., Christian, J., Dunne, J., Gehlen, M., Ilyina, T., John, J. G., Li, H., Long, M. C., Luo, J. Y., Nakano, H., Romanou, A., Schwinger, J., Stock, C., Santana-Falcon, Y., Takano, Y., Tjiputra, J., Tsujino, H., Watanabe, M., Wu, F., and Yamamoto, A.: Tracking Improvement in Simulated Marine Biogeochemistry Between CMIP5 and CMIP6. Curr Clim Change Rep **6,** 95–119, https://doi.org/10.1007/s40641-020-00160-0, 2020.

Takahashi, T., Broecker, W. S., and Langer, S.: Redfield ratio based on chemical data from isopycnal surfaces, J. Geophys. Res., 90, 6907–6924, 1985.

Wanninkhof, R.: Relationship between wind speed and gas exchange over the ocean, J. Geophys. Res., 97, 7373–7382, doi:10.1029/92JC00188, 1992.

Wanninkhof, R.: Relationship between wind speed and gas exchange over the ocean revisited, Limnol. Oceanogr. Methods, 12, 351-362, doi:10.4319/lom.2014.12.351, 2014.

Weiss, R. F., and Price, B. A. : Nitrous oxide solubility in water and seawater Marine Chemistry, Volume 8, Issue 4, Pages 347-359; DOI: 10.1016/0304-4203(80)90024-9, 1980.

B. Supporting figures

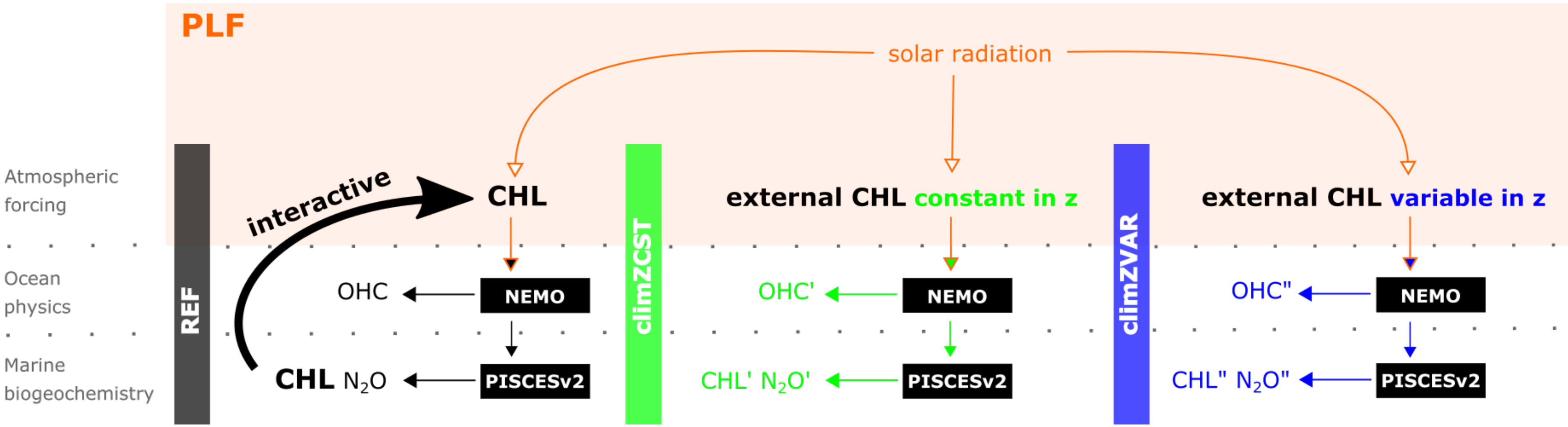

Figure S1: Schematic diagram of the numerical set. The phytoplankton-light feedback (PLF) encompasses the interaction between the incoming solar radiation (identical among the 3 simulations) and the CHL concentration used to filter its penetration through the water column. Different representations of the PLF are distinguished in function of the CHL used to filter the incoming radiation: it is either computed from PISCESv2 model (REF) or externally prescribed from an observed climatology (climZCST and climZVAR). We show that the nature of the CHL chosen to interact with light determines different states of ocean physics (e.g. OHC, temperature, dynamics, stratification) that drive different states of marine biogeochemistry (e.g. N_2O, CHL, O2).

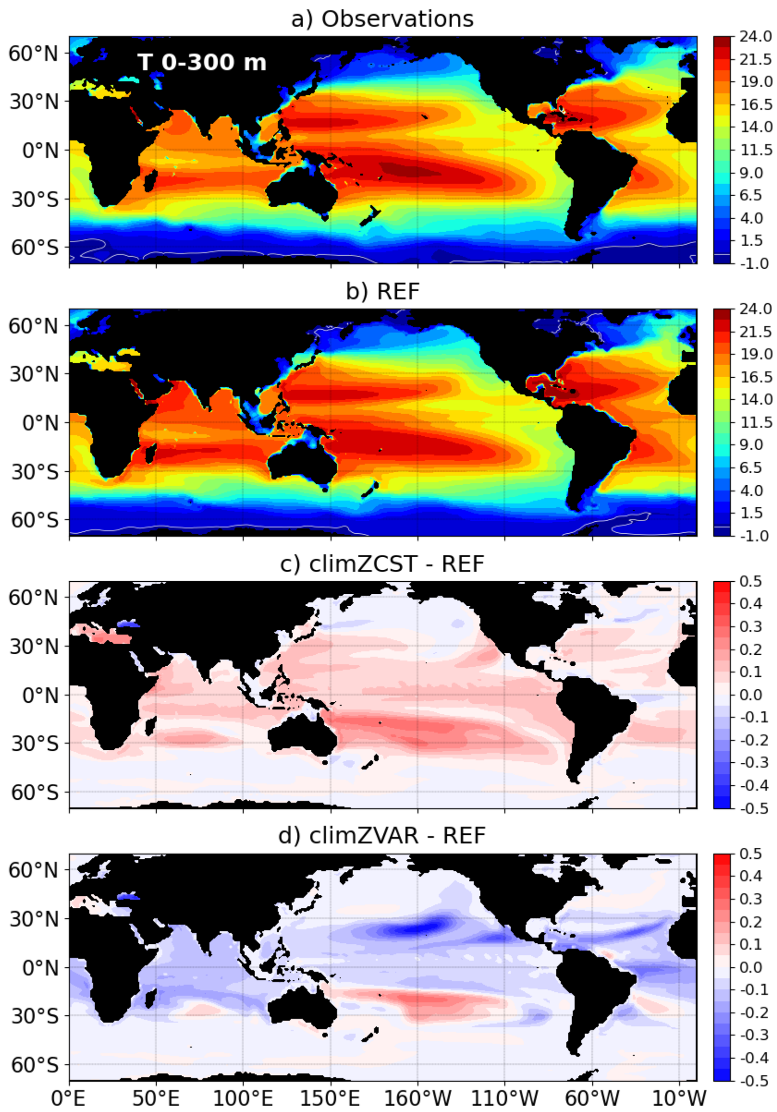

Figure S2: Annual mean temperature (°C) averaged over the 0-300 m ocean layer for the 2009-2018 period. The heat perturbations induced by changing the CHL field interacting with light are mainly restricted in the tropical band (*Figure S2*, c-d).

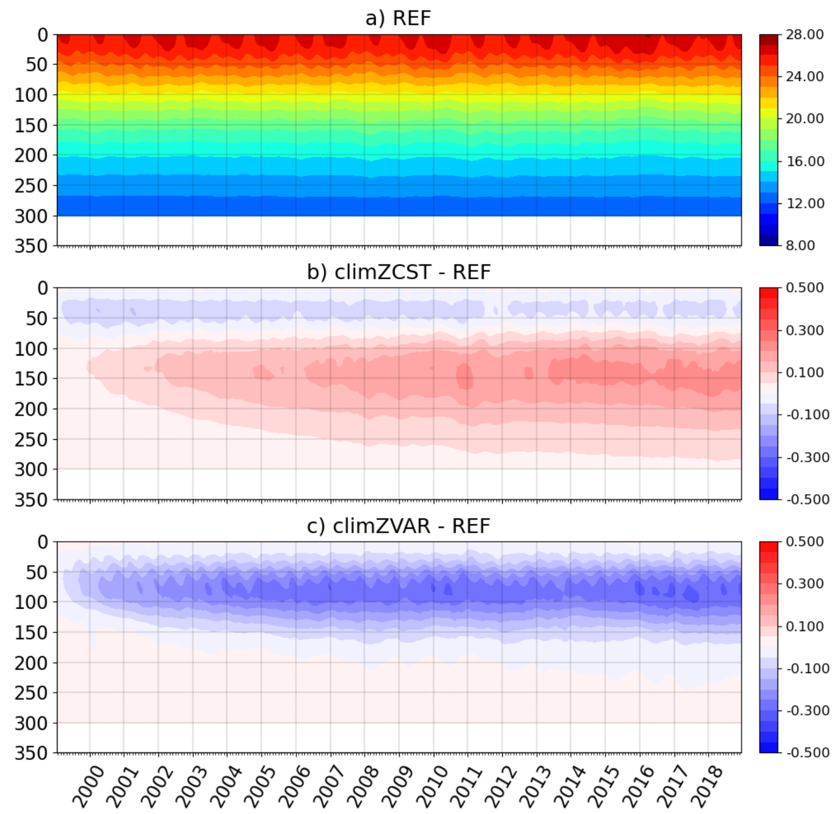

Figure S3: Time-depth diagram of temperature averaged over an extended tropical domain (35°S-35°N) for a) the control experiment REF, and its differences with b) climZCST and c) climZVAR.

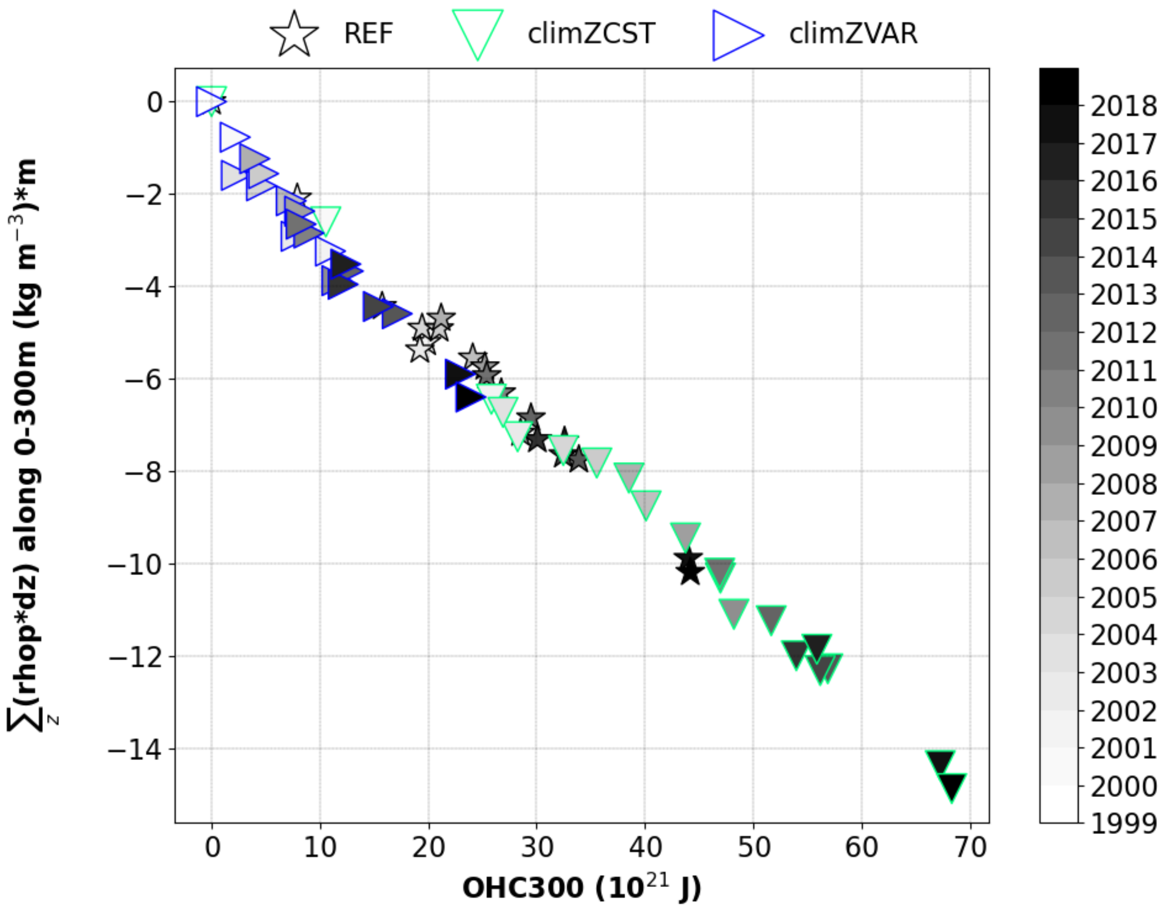

Figure S4: Annual density vertically integrated from 0 to 300 meter depths (kg/m^2) as a function of the annual OHC300 (ZJ) and annually averaged over an extended tropical domain (35°S-35°N). All points reflect anomalies compared to year 1999.

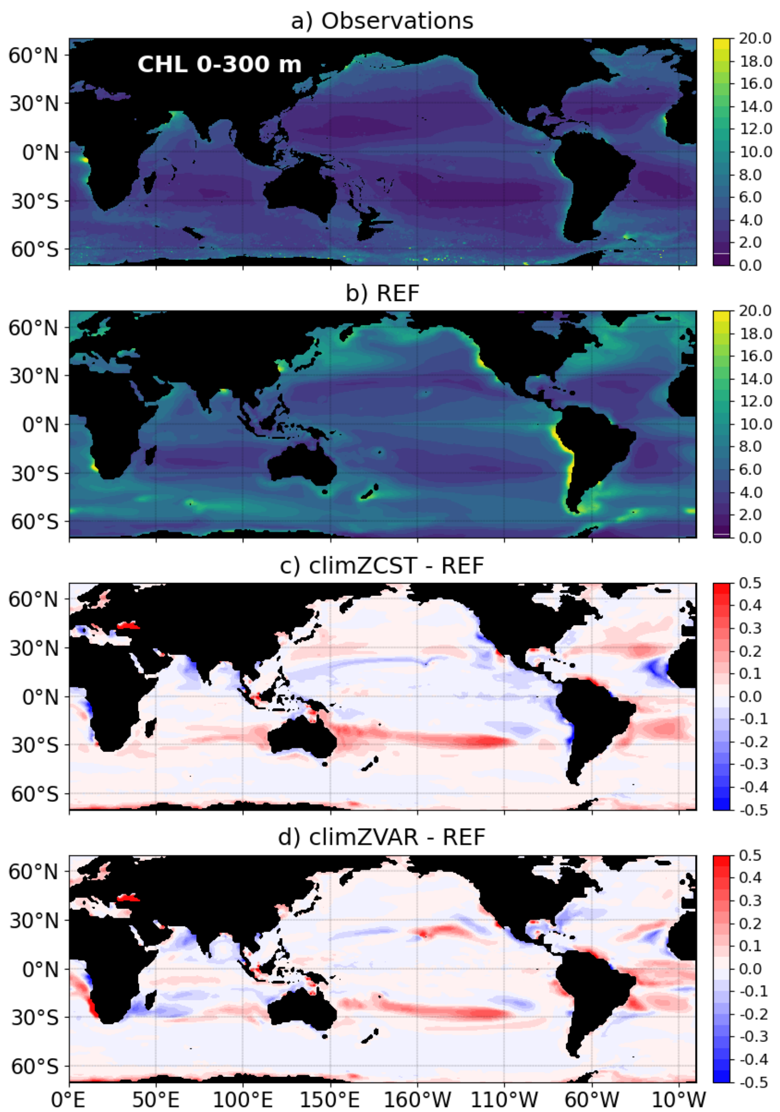

Figure S5: Annual mean of the vertical sum over the 0-300 m ocean layer of CHL concentration (mgCHL m^{-3}) a) observed and b-d) modelled by PISCESv2 for the 2009-2018 period.

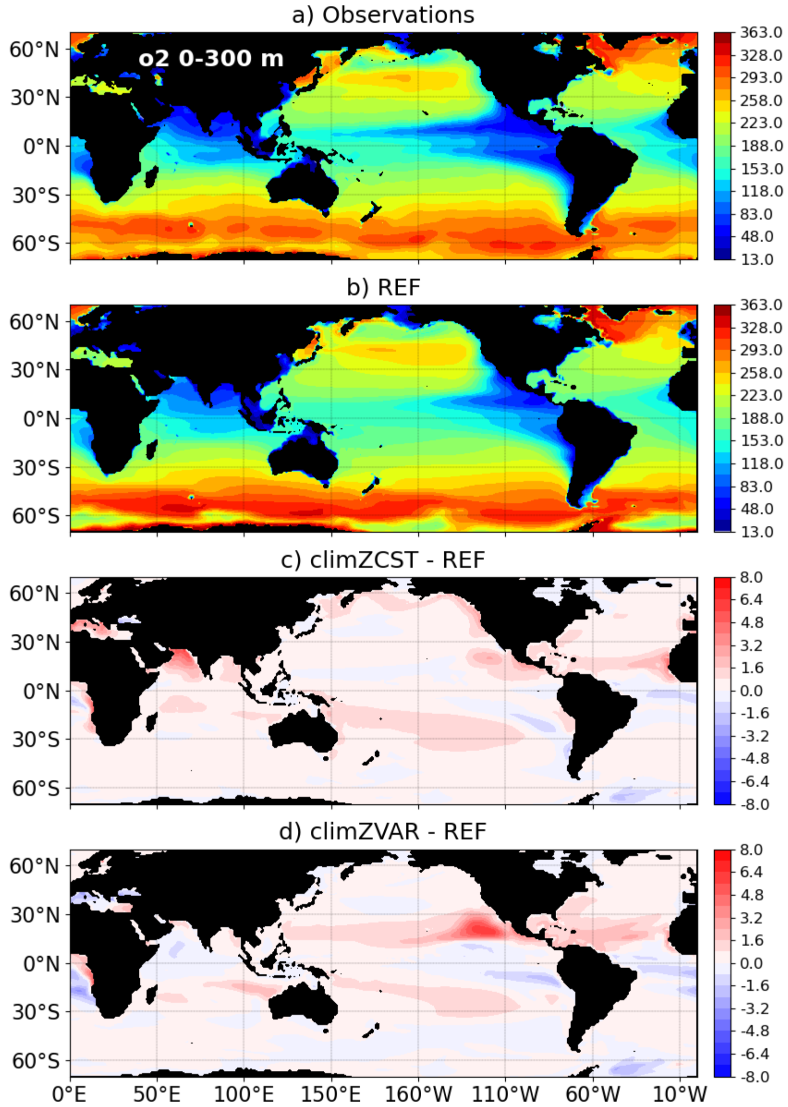

Figure S6: Annual mean oxygen concentration (mmol m^{-3}) averaged over the 0-300 m ocean layer for the 2009-2018 period. An incomplete PLF contributes to overestimate the oxygen concentration in the North Pacific oxygen minimum zone, which in turn leads to a decrease in local N_2O production (Figure 4, e-f).